

Provided for non-commercial research and education use.  
Not for reproduction, distribution or commercial use.



This article appeared in a journal published by Elsevier. The attached copy is furnished to the author for internal non-commercial research and education use, including for instruction at the authors institution and sharing with colleagues.

Other uses, including reproduction and distribution, or selling or licensing copies, or posting to personal, institutional or third party websites are prohibited.

In most cases authors are permitted to post their version of the article (e.g. in Word or Tex form) to their personal website or institutional repository. Authors requiring further information regarding Elsevier's archiving and manuscript policies are encouraged to visit:

<http://www.elsevier.com/copyright>



Contents lists available at ScienceDirect

Earth and Planetary Science Letters

journal homepage: [www.elsevier.com/locate/epsl](http://www.elsevier.com/locate/epsl)

## Spin states and hyperfine interactions of iron in (Mg,Fe)SiO<sub>3</sub> perovskite under pressure

Han Hsu<sup>a,\*</sup>, Koichiro Umemoto<sup>b</sup>, Peter Blaha<sup>c</sup>, Renata M. Wentzcovitch<sup>a</sup>

<sup>a</sup> Department of Chemical Engineering Materials Science, University of Minnesota, Minneapolis, MN 55455, USA

<sup>b</sup> Department of Geology and Geophysics, University of Minnesota, Minneapolis, MN 55455, USA

<sup>c</sup> Institute of Materials Chemistry, Vienna University of Technology, Getreidemarkt 9/165-TC, A-1060 Vienna, Austria

### ARTICLE INFO

#### Article history:

Received 10 September 2009

Received in revised form 3 February 2010

Accepted 18 February 2010

Available online 10 April 2010

Editor: L. Stixrude

#### Keywords:

spin crossover  
intermediate spin  
quadrupole splitting  
iron-bearing  
perovskite  
lower mantle

### ABSTRACT

With the guidance of first-principles phonon calculations, we have searched and found several metastable equilibrium sites for substitutional ferrous iron in MgSiO<sub>3</sub> perovskite. In the relevant energy range, there are two distinct sites for high-spin, one for low-spin, and one for intermediate-spin iron. Because of variable d-orbital occupancy across these sites, the two competing high-spin sites have different iron quadrupole splittings (QS). At low pressure, the high-spin iron with QS of 2.3–2.5 mm/s is more stable, while the high-spin iron with QS of 3.3–3.6 mm/s is more favorable at higher pressure. The crossover occurs between 4 and 24 GPa, depending on the choice of exchange-correlation functional and the inclusion of on-site Coulomb interaction (Hubbard *U*). Our calculation supports the notion that the transition observed in recent Mössbauer spectra corresponds to an atomic-site change rather than a spin-state crossover. Our result also helps to explain the lack of anomaly in the compression curve of iron-bearing silicate perovskite in the presence of a large change of quadrupole splitting, and provides important guidance for future studies of thermodynamic properties of this phase.

© 2010 Elsevier B.V. All rights reserved.

### 1. Introduction

Lower mantle, located between the depth of about 600 km and 2890 km, with pressures and temperatures varying from ~23 to 135 GPa and ~1900 to 4000 K, is the largest region of the Earth's interior. Two major constituents of this region are ferropericlase, (Mg, Fe)O, and iron- and aluminum-bearing magnesium silicate perovskite, (Mg,Fe)(Si,Al)O<sub>3</sub>, with ~35 vol.% and ~62 vol.%, respectively. The valence and spin state of iron directly affect the transport, elastic, and rheological properties of the host phase, as reviewed by Lin and Tsuchiya (2008) and Hsu et al. (in press).

Ferrous iron (Fe<sup>2+</sup>) has six 3d electrons. Its spin state can thus be high-spin (HS), *S* = 2, intermediate-spin (IS), *S* = 1, or low-spin (LS), *S* = 0, where *S* denotes for the quantum number of total spin. While the pressure-induced spin-state crossover in ferropericlase observed experimentally (see Lin and Tsuchiya (2008) for a comprehensive review) has been confirmed to be a HS-to-LS crossover by first-principles calculations (Cohen et al., 1997; Sturhahn et al., 2005; Tsuchiya et al., 2006), its detailed mechanism in (Mg,Fe)(Si,Al)O<sub>3</sub> still remains controversial. This is mainly due to the complexity of the

iron- and aluminum-bearing perovskite. For example, the fraction and the site occupancy of ferric iron is still not well characterized.

Various experimental techniques have been used to study the spin-state crossover in perovskite, including X-ray emission spectroscopy (XES) (Badro et al., 2004; Li et al., 2004), X-ray absorption near-edge spectroscopy (XANES) (Narigina et al., 2009), and Mössbauer spectroscopy (MS) (Jackson et al., 2005; Li et al., 2006; Lin et al., 2008; McCammon et al., 2008). The satellite peak intensity in XES spectra is used to estimate the average spin magnetic moment of iron (Badro et al., 2004; Li et al., 2004). These XES spectra show great similarity in the evolution with increasing pressure, but they were interpreted differently. A two-step spin-state crossover (a sudden change from pure HS to a HS/LS mixture at 70 GPa followed by sudden change from the HS/LS mixture to pure LS at 120 GPa) was suggested by Badro et al. (2004), while the broad crossover was attributed to the existence of IS iron by Li et al. (2004). There were also different interpretations of the Mössbauer spectra in different studies, even though their main results were similar. Using the samples with 10% of iron, two types of ferrous iron with different quadrupole splittings (QS) were found (Jackson et al., 2005; Li et al., 2006). As the pressure increases, the population of ferrous iron with lower QS (2.0–2.8 mm/s) decreases while the population of ferrous iron with higher QS (3.4–3.5 mm/s) increases. However, Jackson et al. (2005) suggested both ferrous iron remain at HS state in the 0–120 GPa range, while Li et al. (2006) suggested spin-state crossover could occur in the ferrous iron.

\* Corresponding author. Tel.: +1 612 624 2872; fax: +1 612 626 7246.  
E-mail address: [hshuhan@cems.umn.edu](mailto:hshuhan@cems.umn.edu) (H. Hsu).

In an attempt to properly interpret these experiments, several calculations for ferrous iron in perovskite have been performed, but they are not always in agreement with each other. The HS-to-LS transition pressure in static calculations strongly depends on the choice of exchange-correlation functional. In general, the generalized-gradient approximation (GGA) gives a transition pressure higher than the local density approximation (LDA) by about 50 GPa (Bengtson et al., 2008; Caracas and Cohen, 2007; Hofmeister, 2006; Stackhouse et al., 2007; Umemoto et al., 2008; Zhang and Oganov, 2006), as have been seen in other systems as well (Tsuchiya et al., 2004; Yu et al., 2007; Yu et al., 2008). Despite such a discrepancy, these calculations do have one thing in common: HS-to-LS crossover is not observed, irrespective of the exchange-correlation functional used in the calculation.

By combining MS and XES spectra, an entirely different spin-state crossover scenario was proposed recently (Lin et al., 2008; McCammon et al., 2008). Similar to other studies adopting MS, two types of ferrous iron were also found, one with QS of 3.5–4.0 mm/s, the other with QS of 2.4 mm/s. McCammon et al. (2008) showed that for pressures lower than ~30 GPa, the low-QS iron dominates; starting at ~30 GPa, the population of high-QS iron increases with pressure at the expense of the low-QS iron. In this study, the high-QS iron was suggested to be in IS state. A HS-to-LS crossover was thus proposed, and it was suggested ferrous iron remains in the IS state in the 30–110 GPa range. It should be pointed out that a high QS in iron does not necessarily imply an IS state. For example, iron in almandine is not in the IS state but still has QS > 3.5 mm/s (Murad and Wagner, 1987). A crossover in the 30–87 GPa range is also observed in XANES (Narigina et al., 2009). Indeed the observed transition pressure agrees with MS spectra, but the spin state of iron cannot be determined from the XANES spectra either.

The nuclear charge distribution in  $^{57}\text{Fe}$  is not spherical. Its multipole expansion has non-vanishing high-order moments. The nuclear quadrupole moment interacts with the electric field resulting from the electrons around the nucleus. The QS is directly proportional to the product of the nuclear quadrupole moment and the electric field gradient (EFG) at the center of the nucleus (Chen and Yang, 2007; Petrilli et al., 1998). In  $(\text{Mg,Fe})\text{SiO}_3$  perovskite, iron substitutes for magnesium in the large 8–12 coordinated cage. It is conceivable that iron might find metastable sites, in addition to the lowest energy site, within the large Mg cage. At each site, the ligand field (and electron charge distribution) is different. Such a difference, even if small, can cause significant differences in the EFG and thus lead to very different QSs, irrespective of spin state. Therefore, interpretation of the spin state on the basis of QSs observed in MS spectra is not unambiguous. At different equilibrium sites, iron in the same spin state may still have different QS.

One of the objectives of this work is to elucidate the dependence of QS on the equilibrium position of iron. The search for possible equilibrium sites of iron in the perovskite cage was carried out by investigating first the vibrational modes with imaginary frequencies in a hypothetical cubic perovskite structure of  $(\text{Mg}_{0.75}\text{Fe}_{0.25})\text{SiO}_3$  with 20 atoms per unit cell. This procedure was used previously in a similar search for sites of iron in the LS state (Umemoto et al., 2008). Because such a structure is unstable, several zone center modes with imaginary frequencies can be found. The atoms in the cubic perovskite were then displaced according to the unstable eigenmodes, followed by a structural optimization. The resulting iron site may be in a stable, metastable, or unstable equilibrium position. An unstable equilibrium site will have further imaginary phonon frequencies, and further structural optimizations must be performed. This procedure is repeated until all phonon frequencies are real. In this way, several metastable atomic structures for ferrous iron in the perovskite cage can be found, and each one of them can lead to a distinct QS. In a recent work (Bengtson et al., 2009), the dependence of QS on the iron site was also demonstrated. The difference between our work and Bengtson et al. (2009) will be discussed later.

The on-site Coulomb interaction is usually not negligible in transition metal oxides. In addition to standard density functional theory (DFT) method, the calculations using DFT +  $U$  method are also presented in this paper. Instead of treating the Hubbard  $U$  as a fitting parameter, we calculated  $U$  by first principles. The first-principles Hubbard  $U$  is spin- and structure-dependent, as has been shown in many previous calculations (Cococcioni and de Gironcoli, 2005; Hsu et al., 2009; Tsuchiya et al., 2006) and shall be also shown in this work. The effect of Hubbard  $U$  on transition pressure and QS will be demonstrated.

This paper is organized as follows. In Section 2, we describe details of the calculations. In Section 3, we detail the procedure used to search for equilibrium sites and discuss how the QS is affected. Since the results are sensitive to the iron concentration and the electronic structure method, both pseudopotential and all-electron methods are used. In Section 4, the dependence of transition pressure on iron concentration, exchange-correlation functional, and on-site Coulomb interaction is discussed. In Section 5 we state our conclusions.

## 2. Computational details

Our structural optimizations are performed using damped variable cell shape molecular dynamics (Wentzcovitch et al., 1993), and the phonon calculations are based on density functional perturbation theory (DFPT) (Baroni et al., 2001). Both features are included in the QUANTUM-ESPRESSO package (Giannozzi et al., 2009). Both the LDA and GGA (Perdew et al., 1996) are adopted. The Hubbard  $U$  is determined from the LDA and GGA ground states using linear response theory (Cococcioni and de Gironcoli, 2005). The pseudopotentials of Fe, Si, and O are generated by Vanderbilt's method (Vanderbilt, 1990) with valence electronic configurations of  $3s^23p^63d^{6.5}4s^14p^0$ ,  $3s^23p^1$ , and  $2s^22p^4$ , and core radii (for all quantum numbers  $l$ ) of 1.8, 1.6, and 1.4 a.u., respectively. The pseudopotential of Mg is generated by von Barth–Car's method. Five configurations,  $3s^23p^0$ ,  $3s^13p^1$ ,  $3s^13p^0.53d^{0.5}$ ,  $3s^13p^{0.5}$ , and  $3s^13d^1$ , are used, with decreasing weights 1.5, 0.6, 0.3, 0.3, and 0.2, respectively. Core radii for all quantum numbers  $l$  are 2.5 a.u. The energy cutoff is 40 Ry for the wave function and 160 Ry for the charge density. When performing structural optimization,  $4 \times 4 \times 2$  and  $2 \times 2 \times 2$  k-point grids are used for 20- and 40-atom cells, respectively. The structural optimizations are terminated when interatomic forces are smaller than  $2 \times 10^{-4}$  Ry/a.u. Finer k-point grids ( $4 \times 4 \times 4$ ) are used in the calculations of density of states (DOS) for 40-atom cells. The compression curves are fitted to the 3 rd-order Birch–Murnaghan equation of states. The EFGs are calculated using the augmented plane wave + local orbitals (APW + lo) method (Madsen et al., 2001) implemented in the WIEN2k code (Blaha et al., 2001). They are converted to the QS values using iron nuclear quadrupole moment  $Q = 0.16$  barn (Petrilli et al., 1998). It should be noted that slightly larger  $Q$  values are discussed in literature, and using  $Q = 0.18$  barn would increase all calculated QS by 13%.

## 3. Atomic structure and quadrupole splitting

We started our search of the HS iron equilibrium sites in  $(\text{Mg}_{0.75}\text{Fe}_{0.25})\text{SiO}_3$  20-atom cells (25% of iron concentration) using GGA. As shown in Umemoto et al. (2008), the GGA equilibrium volume of HS  $(\text{Mg}_{0.75}\text{Fe}_{0.25})\text{SiO}_3$  is 286.24 a.u.<sup>3</sup>/f.u. (1144.97 a.u.<sup>3</sup> per 20-atom cell). A hypothetical cubic perovskite cell with equal volume was generated, and its phonon frequencies and zone center normal modes were calculated. Among its seven distinct soft modes, three of them can lead to stable perovskite structures, directly or indirectly, as detailed below. These three structures (at 0 GPa) are shown in Fig. 1, where the bigger (yellow) spheres at the center of each panel represent iron, the smaller (green) spheres represent magnesium, and the numbers in parenthesis are the respective QSs of iron nuclei.

The HS state with QS of 3.3 mm/s is produced directly from the mode with the lowest negative energy (imaginary frequency  $\omega = i375.56 \text{ cm}^{-1}$ ). This mode corresponds to the out-of-phase

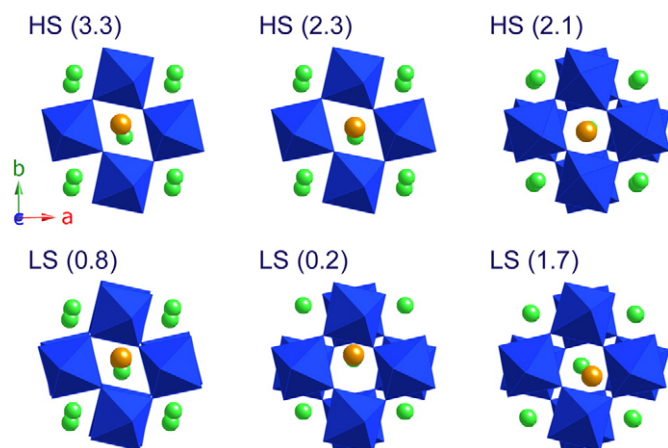


**Fig. 1.** The atomic structures of the HS and LS ( $\text{Mg}_{0.75}\text{Fe}_{0.25}\text{SiO}_3$ ) perovskite at 0 GPa viewed along the [001] direction. Numbers in the parentheses are quadrupole splittings (QS) (in mm/s) of the iron nucleus in each configuration. The bigger (yellow) spheres at the center of each panel are iron, the smaller (green) spheres are magnesium. The main difference between the two competing HS states (with QS of 3.3 and 2.3 mm/s) is the equilibrium position of iron. See Table 1.

rotation of the Si–O octahedra about the [100] direction of the cubic perovskite. In fact, the atomic structure of this HS state is the same as the one presented in Umemoto et al. (2008). The HS state with QS of 2.3 mm/s is produced by the mode with imaginary frequency  $\omega = i120.42 \text{ cm}^{-1}$ . This mode, instead of octahedral rotation, corresponds to a horizontal displacement of magnesium and Si–O octahedral array along the  $xy$  plane. The atomic structures of these two HS states show great resemblance, including the position of magnesium and the tilting of the Si–O octahedra. The main difference between them is the position of iron. By moving the iron from the site that produces QS of 3.3 mm/s along the [100] and  $[0\bar{1}0]$  directions sequentially (not exactly the  $[1\bar{1}0]$  direction) and performing structural optimization after such displacing, the HS state with QS of 2.3 mm/s can be produced. In both states, the irons lie on the horizontal mirror plane. It should be mentioned that the QS of 2.3 mm/s is obtained from ( $\text{Mg}_{0.875}\text{Fe}_{0.125}\text{SiO}_3$ ) (12.5% iron concentration) instead of ( $\text{Mg}_{0.75}\text{Fe}_{0.25}\text{SiO}_3$ ). This is because in WIEN2k, the HS iron with QS of 2.3 mm/s can be stabilized only in ( $\text{Mg}_{0.875}\text{Fe}_{0.125}\text{SiO}_3$ ). In QUANTUM-ESPRESSO, both types of HS states can be stabilized in both iron concentrations, and their atomic and electronic structures are not sensitive to the iron concentration.

The HS state with QS of 2.1 mm/s is produced by a two-step procedure. Applying the phonon mode with imaginary frequency  $\omega = i371.37 \text{ cm}^{-1}$  to the cubic perovskite followed by a structural optimization produces an unstable structure with one soft mode  $\omega = i262.64 \text{ cm}^{-1}$ . Applying this soft mode to the present unstable structure lead to the metastable structure with QS of 2.1 mm/s. From the octahedral tilting shown in Fig. 1, we can clearly see the effect of the two rotations associated with this structure.

The LS states are also obtained by the guidance of the phonon modes with imaginary frequencies in cubic LS ( $\text{Mg}_{0.75}\text{Fe}_{0.25}\text{SiO}_3$ ) (unit-cell volume  $1137.75 \text{ a.u.}^3$ ). In contrast with the HS case, none of the soft phonon modes can directly produce the final structures shown in Fig. 1. Indeed, the imaginary mode corresponding to the Si–O octahedral

rotations about the [100] direction ( $\omega = i368.67 \text{ cm}^{-1}$ ) produces a structure that resembles the atomic structure of HS state with QS of 3.3 mm/s. However, one imaginary phonon frequency can still be found in this LS state. This mode corresponds to the displacement of iron along the [001] direction. Therefore, the LS iron with QS of 0.8 mm/s is not on the horizontal mirror plane. The other two LS states are produced by two different octahedral rotations, as can be seen in Fig. 1.

Zero pressure volumes and energies of all these states are shown in Table I. The HS states with QS of 2.3 and 3.3 mm/s have similar volumes and energies. The HS state with QS of 2.3 mm/s has larger volume, and its energy is lower than that of HS state with QS of 3.3 mm/s by 1.8 mRy/Fe (24.3 meV/Fe). This energy difference is larger than that presented in Bengtson et al. (2009), most likely due to the difference in the atomic structure obtained in both calculations, as shall be discussed in the next paragraph.

The two competing HS states deserve a closer look. Fig. 2 shows the atomic arrangements around iron in these two states. The  $[0\bar{1}0]$  direction is pointing out of the paper. In both cases, irons lie on the  $xy$  mirror plane, as can be seen from the fact that oxygens above and below the mirror plane are equidistant from iron. On the contrary, in Bengtson et al. (2009), the positions of both HS irons are not exactly on  $xy$  mirror plane. By displacing the HS iron with QS of 3.3 mm/s from its equilibrium site along the [001] and  $[0\bar{1}0]$  directions sequentially to the equilibrium site that causes a QS of 2.3 mm/s, two of the Fe–O distances increase strongly (0.26 Å), one decreases by 0.12 Å, and others barely change.

As described earlier, the QS of iron nucleus is not determined by the spin state, but by the asymmetry of electron charge distribution around the iron nucleus. Because of the different Fe–O arrangements (as shown in Fig. 2), the ligand fields around the two HS iron sites differ as well. This changes the d-orbital occupancies of iron and determines their respective EFGs. In Figs. 3 and 4, the total density of states (DOS) and the projected density of states (PDOS) of the two competing HS states in ( $\text{Mg}_{0.875}\text{Si}_{0.125}\text{SiO}_3$ ) at 0 GPa are plotted. Both HS states are semiconducting with an energy gap slightly larger than 0.1 eV. The difference is mainly on the PDOS of iron. For HS irons, the spin-up electrons occupy all five d-orbitals, and their contribution to the EFG is negligible because the charge distribution is essentially spherical. The EFG results primarily from the spin-down electrons. The main EFG component  $V_{zz}$  depends on the orbital occupancy based on  $V_{zz} \propto e(2n_{xy} - n_{yz} - n_{xz} - 2n_z^2 + 2n_{x^2-y^2}) / r^3$  (Chen and Yang, 2007), where  $n_{xy}, n_{yz}, \dots$  denote for the occupancy of orbitals  $d_{xy}, d_{yz}, \dots$ , respectively, and they can be calculated by integrating PDOS over energy. This expression of  $V_{zz}$  indicates that electrons occupying  $d_{xy}, d_{x^2-y^2}$ , or  $d_z$  orbitals contribute twice as much to the EFG as the  $d_{xz}$  or  $d_{yz}$  electrons. The spin-down occupancies in the HS iron with QS of 3.3 mm/s are  $n_{x^2-y^2} \approx 0.47$  and  $d_{xy} \approx 0.62$ , while the HS iron with QS of 2.3 mm/s has spin-down  $n_{yz} \approx 0.97$ . The other orbitals have negligible occupancies. This difference in the d-orbital occupancy is the origin of the different QSs of the HS iron at different sites.

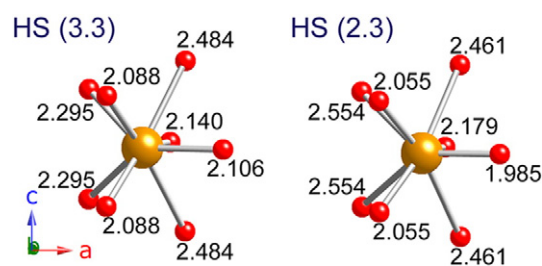


**Fig. 2.** Local atomic configurations around iron in the two competing HS states at 0 GPa. Numbers in parentheses are the QSs (in mm/s) of iron. Numbers next to oxygens are Fe–O distances (in Å). While irons are on the  $xy$  mirror plane in both cases, the Fe–O distances (and the resulting ligand fields) are different. The  $[0\bar{1}0]$  direction is pointing outward to the paper.

**Table 1**

The unit-cell volumes ( $V$ ) and relative energies ( $\Delta E$ ) of ( $\text{Mg}_{0.75}\text{Fe}_{0.25}\text{SiO}_3$ ) in various states at 0 GPa. Numbers in parentheses are the corresponding QSs of iron nuclei.

	HS (3.3)	HS (2.3)	HS (2.1)	LS (0.8)	LS (0.2)	LS (1.7)
$V$ ( $\text{a.u.}^3/\text{Fe}$ )	1144.97	1147.13	1163.60	1137.75	1166.39	1171.99
$\Delta E$ (mRy/Fe)	0	−1.8	51.9	85.2	53.6	194.1



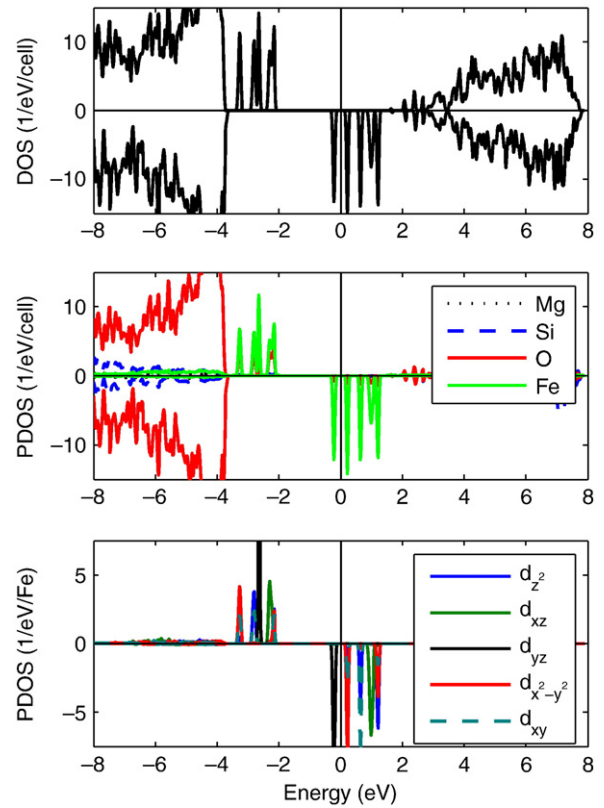
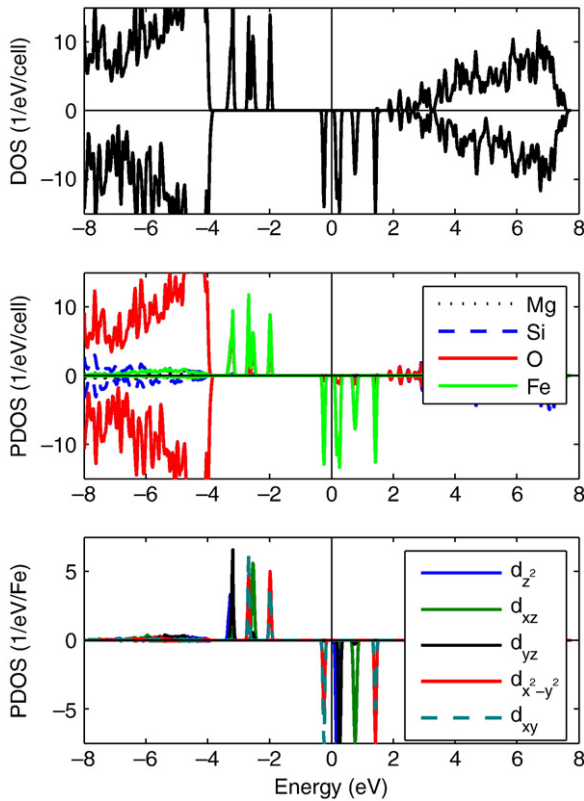


**Fig. 3.** Density of states of HS ( $\text{Mg}_{0.875}\text{Fe}_{0.125}$ ) $\text{SiO}_3$  with QS of 3.3 mm/s at 0 GPa. The energy gap is a little bit larger than 0.1 eV. Spin-down electrons occupy  $d_{xy}$  and  $d_{x^2-y^2}$  orbitals.

**Fig. 4.** Density of states of HS ( $\text{Mg}_{0.875}\text{Fe}_{0.125}$ ) $\text{SiO}_3$  with QS of 2.3 mm/s at 0 GPa. The energy gap is a little bit larger than 0.1 eV. Spin-down electrons occupy  $d_{yz}$  orbital.

The approach to find stable IS iron sites in perovskite is different from that of finding HS and LS sites. The reason is, IS iron cannot be stabilized in the hypothetical cubic perovskite, and this hinders the phonon calculation. Without the guidance from the soft phonon modes, an alternative approach was adopted. We displaced iron from the HS equilibrium sites on the mirror plane along the [001] direction (P1 symmetry) and performed structural optimization subsequently. The atomic structures of the two competing HS states were used as the starting configuration, and the same IS site was obtained. The magnetic moment of iron can be stabilized to  $S=1$  spontaneously without applying any constraint when  $P \geq 30$  GPa. Therefore, results for IS irons are reported only above 30 GPa. The IS state can be stabilized using both pseudopotential and all-electron methods. The atomic structure of the IS state presented in this manuscript is the same as the one presented in Umemoto et al. (2009).

The QSs of iron nuclei in the three HS, three LS, and one IS states at different pressures are shown in Fig. 5. They are not very sensitive to pressure. Below 120 GPa, HS irons have  $QS > 2.0$  mm/s, while LS and IS irons have  $QS < 2.0$  mm/s. In our calculation, the atomic structures of the two competing HS states remain distinct in the 0–120 GPa range, but become indistinguishable at 150 GPa. In Bengtson et al. (2009), the two HS states become indistinguishable at 60 GPa. At 30 GPa the IS state cannot be stabilized with 25% iron concentration. The QS of IS iron at 30 GPa is obtained with 12.5% of iron while at other pressures with 25% of iron.

#### 4. Exchange-correlation functional, Hubbard $U$ , and transition pressure

The enthalpies of ( $\text{Mg}_{0.75}\text{Fe}_{0.25}$ ) $\text{SiO}_3$  in various spin states with various iron nuclear QS are plotted in Fig. 6, where the enthalpy of the HS state with QS of 3.3 mm/s is used as a reference. It is quite obvious

that among the three LS and three HS states, only the LS state with QS of 0.8 mm/s and the two competing HS states with QS of 2.3 and 3.3 mm/s are relevant. These three states are referred to as LS, low-QS HS and high-QS HS, respectively, in the rest of the paper. The other three states associated with two octahedral rotations are in a higher energy range. In the entire pressure range investigated, the IS state has greater enthalpy than the LS, low-QS, and high-QS HS states. Neither HS-to-IS nor HS-to-LS crossover occurs. A transition between the two

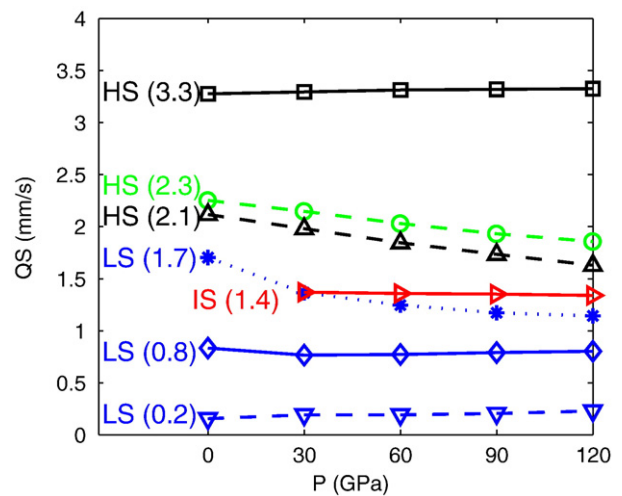


**Fig. 5.** Quadrupole splitting of iron nucleus versus pressure. Numbers in the parentheses are the QS at 0 GPa. The QS of IS iron at 30 GPa and the HS iron with 2.3 mm/s are obtained using 12.5% iron concentration.

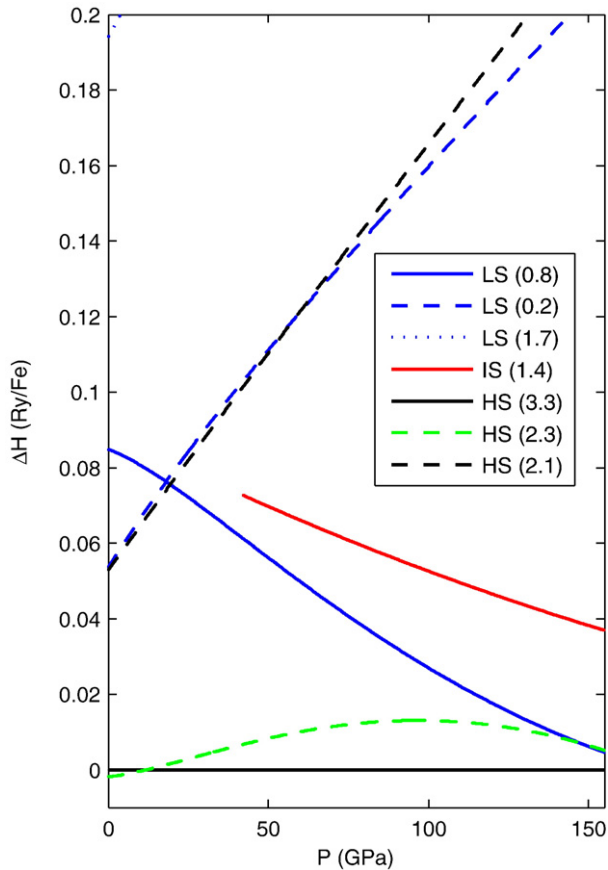


**Fig. 6.** The enthalpies of  $(\text{Mg}_{0.75}\text{Fe}_{0.25})\text{SiO}_3$  in various spin states with various iron nucleus QS, where the enthalpy of the HS state with QS of 3.3 mm/s is used as a reference. The crossover between the two competing HS states occurs at 12 GPa. Neither HS-to-IS nor HS-to-LS crossover occurs in the entire 0–150 GPa range.

competing HS states occurs at 12 GPa. For pressures below 12 GPa, the low-QS HS iron is favored, while the high-QS HS iron is favored above 12 GPa. In the 0–60 GPa range, the low-QS HS state has lower energy than the high-QS HS state. The greater volume of the former contributes to enthalpy crossing ( $\Delta H = \Delta E + P\Delta V$ ) at 12 GPa. For

lower iron concentrations, the effect of the  $P\Delta V$  term is less significant, and the transition pressure increases, as shall be seen later in the results for 12.5% of iron.

*In situ* X-ray diffraction reveals that iron-bearing perovskite compress anisotropically. The *Pbnm* *b*-axis is anomalously robust compared with the *a*- and *c*-axes. This difference in axial compressibility was suggested to be a signature of the stabilization of IS state in the perovskite cage (McCammon et al., 2008). However, as shown in Fig. 7, the *b*-axis of both HS ( $\text{Mg}_{0.75}\text{Fe}_{0.25})\text{SiO}_3$  and  $\text{MgSiO}_3$  are much less compressible than the *a*- and *c*-axes. Anisotropic compressibility is not related to the stabilization of the IS state or to the HS-to-IS crossover. Throughout the low- to high-QS crossover, anisotropy remains essentially unchanged. As already shown in Fig. 1, only the iron position changes in the 8–12 coordinated cage, while the other atomic positions remain essentially unchanged. This might hinder the detection of the iron displacement using *in situ* X-ray diffraction. The change in iron position might be more readily detected by XANES experiments.

To demonstrate the dependence of transition pressure on iron concentration and on-site Coulomb interaction, both DFT and DFT + *U* calculations were performed for  $(\text{Mg}_{0.875}\text{Fe}_{0.125})\text{SiO}_3$  (12.5% of iron). Fig. 8 shows the Hubbard *U* of iron in  $(\text{Mg}_{0.875}\text{Fe}_{0.125})\text{SiO}_3$  obtained from the GGA and LDA ground states. For all spin states, the Hubbard *U* decreases with volume. The Hubbard *U* obtained from LDA is larger than that obtained from GGA by 0.1–0.2 eV at any given unit-cell volume. In both cases, the LS iron has the largest *U*, while the two HS iron have the smallest (and almost the same) *U*. This is different from the (Mg,Fe)O, in which the HS Fe has larger Hubbard *U* than the LS iron (Tsuchiya et al., 2006). Such a discrepancy may be resolved when the Hubbard *U* is determined in a more rigorous self-consistent approach. In this approach, the Hubbard *U* is determined from the linear response of a series of DFT + *U* ground states (with a series of trial *U* values) to the local perturbation until a consistent result is achieved (Kulik et al., 2006).

Fig. 9 shows the relative enthalpies of LS, IS, and low-QS HS with respect to high-QS HS  $(\text{Mg}_{0.875}\text{Fe}_{0.125})\text{SiO}_3$  in GGA(+*U*) and LDA (+*U*) calculation. In GGA, the crossover between the two competing HS states occurs at 24 GPa, similar to the experimental result in McCammon et al. (2008). Agreeing with  $(\text{Mg}_{0.75}\text{Fe}_{0.25})\text{SiO}_3$ , neither HS-to-LS nor HS-to-IS crossover occurs. After the Hubbard *U* is applied, the relative enthalpies of IS and LS states with respect to HS states increases significantly. Since LS iron has the largest *U*, its enthalpy is shifted further than that of the IS iron. This is the reason why LS iron is less favorable than the IS iron in GGA + *U*. Although the

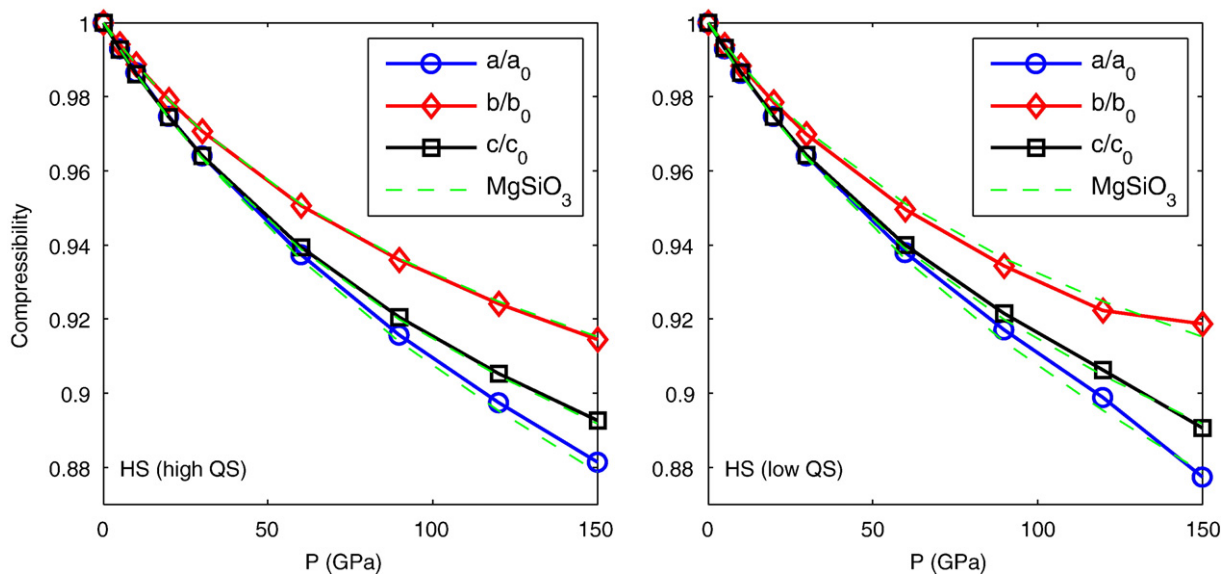


**Fig. 7.** Axial compressibilities of the two competing HS  $(\text{Mg}_{0.75}\text{Fe}_{0.25})\text{SiO}_3$  structures. Both cases show strong anisotropic compressibilities. The *Pbnm* *b*-axis is less compressible than the *a*- and *c*-axes.

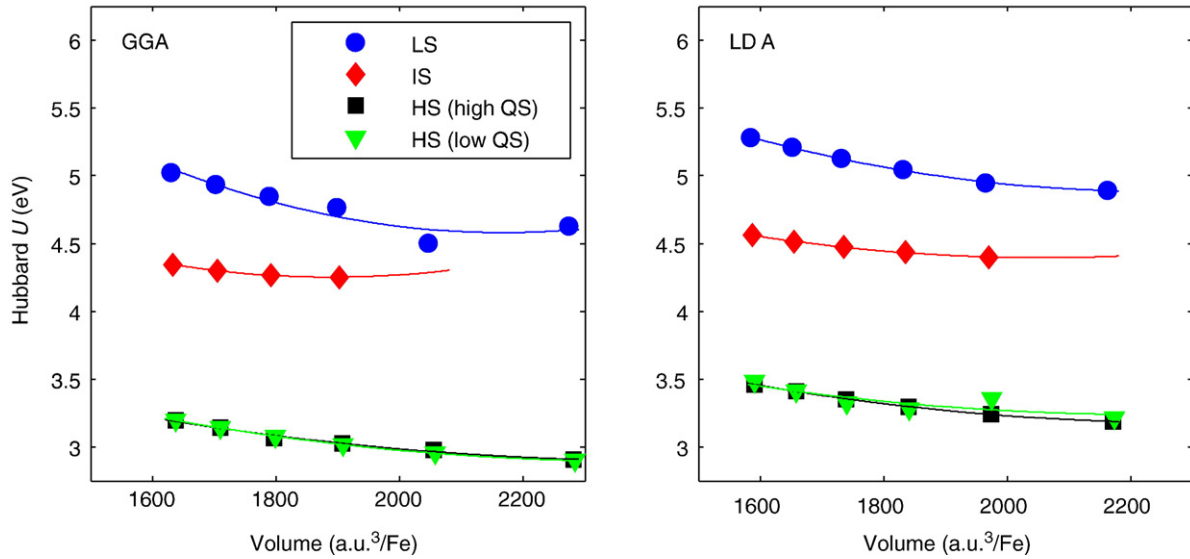


Fig. 8. Hubbard  $U$  of iron in  $(\text{Mg}_{0.875}\text{Fe}_{0.125})\text{SiO}_3$  perovskite obtained from the GGA and LDA ground states at different volumes. For all spin states,  $U$  decreases with volume. The two types of HS Fe have the same  $U$ .

IS iron is more stable than the LS iron in GGA +  $U$ , HS-to-IS crossover still does not occur. The two competing HS state persist in the presence of  $U$ , and the crossover occurs at 15 GPa.

The calculated iron nuclear QS is also affected by the inclusion of Hubbard  $U$ . The calculated QSs of the two competing HS irons become 2.4 and 3.5 mm/s when the Hubbard  $U$  evaluated from the GGA

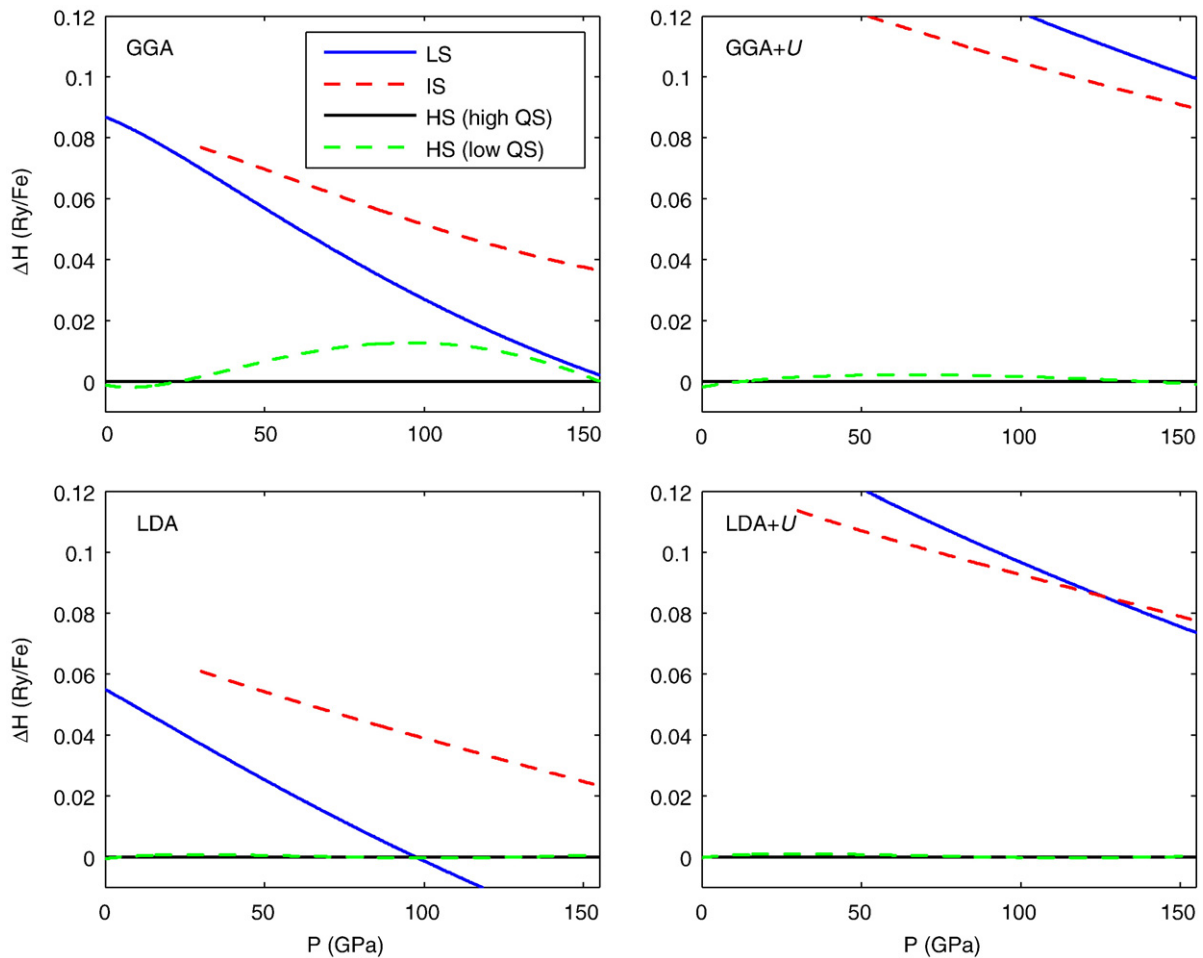


Fig. 9. Relative enthalpies of LS, IS, and low-QS HS  $(\text{Mg}_{0.875}\text{Fe}_{0.125})\text{SiO}_3$  with respect to the high-QS HS state. The crossover from low- to high-QS HS state occurs at 24, 15, 7, and 4 GPa in GGA, GGA +  $U$ , LDA, and LDA +  $U$ , respectively. HS-to-IS crossover does not occur. HS-to-LS crossover occurs at 100 GPa in LDA, and it does not occur in lower-mantle pressure range when GGA, GGA +  $U$ , or LDA +  $U$  is adopted.

ground state (2.9 eV at 0 GPa) is adopted. To further investigate the effect of Hubbard  $U$  on QS, we also calculated the QSs using  $U = 5.8$  eV as a test. The QSs increase to 2.5 and 3.6 mm/s, respectively. In short, the computed QS values are in better agreement with experiments (Jackson et al., 2005; Li et al., 2006; McCammon et al., 2008) when the Hubbard  $U$  is included.

In LDA and LDA +  $U$ , the enthalpy crossing between the two HS states occurs at 7 and 4 GPa, respectively, as shown in Fig. 9. Again, the HS-to-IS crossover does not occur. The transition pressure obtained using LDA is lower than that obtained using GGA. This can be rationalized by the fact that LDA tends to underestimate the “static” volume at a given pressure while GGA tends to overestimate. In LDA, the low-to-high-QS enthalpy crossing occurs at 7 GPa. The static volumes of the low- and high-QS HS states at this pressure are 2122 and 2121 a.u.<sup>3</sup>/Fe. In GGA, the two competing HS states with these volumes correspond to 20 GPa, in agreement with the calculated transition pressure of 24 GPa.

In our calculations, we considered the simplest case, the uniformly distributed ferrous irons in ferromagnetic state. In experiments, the spatial distribution of iron may not be uniform and their magnetic moments may not be ferromagnetically aligned. However, it appears that the effect of disorder on the QSs is small, since our calculations reproduce experimental QSs quite well. The site-change pressure might vary locally with atomic ordering, as shown in Umemoto et al. (2008), for the case of spin-transition pressures, but this pressure also varies from method to method. An assessment of the true effect of ordering is indeed important but not an easy task given the sensitivity to methodology utilized. Therefore, we do not study different atomic configurations in this work. We restrict ourselves to demonstrating that the phenomenon of site change and the QSs associated with these sites is independent of the method of calculation. Even with the simplest atomic configuration, our calculations still showed the complexity of (Mg,Fe)SiO<sub>3</sub>. The LDA calculation agrees with the XES data interpreted by Badro et al. (2004), where HS-to-IS crossover can happen at about 100 GPa. The GGA and GGA +  $U$  calculations reproduce the measured QS in Jackson et al. (2005), Li et al. (2006), and McCammon et al. (2008), and also show agreement with the crossover from the low- to high-QS observed in these experiments. None of the calculations supports the HS-to-IS interpretation proposed by McCammon et al. (2008), and three of them (GGA, GGA +  $U$ , and LDA +  $U$ ) support the interpretation by Jackson et al. (2005), namely, ferrous iron stay in HS state in 0–120 GPa. The calculation of XES spectra, especially the  $K\beta$  peak and its satellite  $K\beta'$ , can be expected to provide a more conclusive result. However, the  $K\beta$  peak, associated with 1 s hole filled by a 3p electron, is dominated by atomic multiplet effects, and such spectroscopy can hardly be described by any single-electron theory, for example, DFT. Nevertheless, we can still expect that the two competing HS irons lead to different  $K\beta'$  intensities, due to their different d-orbital occupancies.

## 5. Conclusion

Using unstable zone center phonon modes of the cubic iron-bearing magnesium silicate perovskite as guidance, several equilibrium sites for ferrous iron in the perovskite cage of MgSiO<sub>3</sub> were found. Their energies are grouped in two different ranges, based on the tilting of Si–O octahedra. In the relevant (lower) energy range, there is one site for low-spin, one for intermediate-spin, and two for high-spin iron. The position of magnesium and the tilting of Si–O octahedra in these two HS states are essentially the same. The main difference is the equilibrium position of iron.

The quadrupole splittings (QS) at the iron nuclei and enthalpies of all equilibrium structures were calculated. In all cases, the QSs are not very sensitive to pressure. Due to different d-orbital occupancies caused by different ligand fields at different sites, the iron at the two HS sites have very different QSs, i.e., 3.3–3.6 and 2.3–2.5 mm/s. These

two HS states compete energetically. The enthalpy crossing from the low- to high-QS HS states occurs in the 4–24 GPa range, depending on the iron concentration, the choice of exchange-correlation functional, and the inclusion of on-site Coulomb interaction (Hubbard  $U$ ). The atomic structures of these two HS states show great resemblance. This makes it difficult to detect the change in iron position through the low- to high-QS crossover in X-ray diffraction.

Within the entire investigated pressure range, the HS-to-IS crossover is never observed, regardless of the iron concentration (12.5% and 25%), the exchange-correlation functional (LDA and GGA), and the inclusion of Hubbard  $U$ . The computed QSs of the two HS irons agree with the QS observed in Mössbauer spectra, while the computed QS of IS iron (1.4 mm/s) does not. Our calculations therefore support the notion that the crossover around 30 GPa observed in Mössbauer spectra is more likely to be an atomic-site change rather than a spin-state transition.

## Acknowledgements

We thank Catherine McCammon for useful comments on almandine. This work was supported primarily by the MRSEC Program of the National Science Foundation under Award Number DMR-0212302 and DMR-0819885. It was also partially supported by NSF grants ITR-0426757 (VLab), ATM-0426757, and EAR-0815446. PB was supported by the Austrian Science Fund (P20271-N17). Calculations were performed at the Minnesota Supercomputing Institute (MSI).

## References

- Badro, J., Rueff, J., Vanko, G., Monaco, G., Fiquet, G., Guyot, F., 2004. Electronic transitions in perovskite: possible nonconvecting layers in the lower mantle. *Science* 305, 383–386.
- Baroni, S., de Gironcoli, S., Dal Corso, A., Giannozzi, P., 2001. Phonons and related crystal properties from density-functional perturbation theory. *Rev. Mod. Phys.* 73, 515–562.
- Bengtson, A., Persson, K., Morgan, D., 2008. Ab initio study of the composition dependence of the pressure-induced spin crossover in perovskite (Mg<sub>1-x</sub>Fe<sub>x</sub>)SiO<sub>3</sub>. *Earth Planet. Sci. Lett.* 265, 535–545.
- Bengtson, A., Li, J., Morgan, D., 2009. Mössbauer modeling to interpret the spin state of iron in (Mg, Fe)SiO<sub>3</sub>. *Geophys. Res. Lett.* 36, L15301.
- Blaha, P., Schwarz, K., Madsen, G.K.H., Kvasnicka, D., Luitz, J., 2001. In: Schwarz, K. (Ed.), WIEN2k, An Augmented Plane Wave + Local Orbitals Program for Calculating Crystal Properties. Techn. Universität Wien, Vienna.
- Caracas, R., Cohen, R., 2007. Effect of chemistry on the physical properties of perovskite and post-perovskite. In: Hirose, K., Brodholt, J., Lay, T., Yuen, D. (Eds.), Post-perovskite: The Last Mantle Phase Transition, Geophysical Monograph, 174. AGU, Washington D.C.
- Chen, Y.-L., Yang, D.-P., 2007. Mössbauer Effect in Lattice Dynamics. Wiley-VCH, Weinheim.
- Cococcioni, M., de Gironcoli, S., 2005. Linear response approach to the calculation of the effective interaction parameters in the LDA +  $U$  method. *Phys. Rev. B* 71, 035105.
- Cohen, R.E., Mazin, I.I., Isaak, D.G., 1997. Magnetic collapse in transition metal oxides at high pressure: implications for the Earth. *Science* 275, 654–657.
- Giannozzi, P., Baroni, S., Bonini, N., Calandra, M., Car, R., Cavazzoni, C., Ceresoli, D., Chiarotti, G.L., Cococcioni, M., Dabo, I., Dal Corso, A., de Gironcoli, S., Fabris, S., Fratesi, G., Gebauer, R., Gerstmann, U., Gougoussis, C., Kokalj, A., Lazzeri, M., Martin-Samos, L., Marzari, N., Mauri, F., Mazzarello, R., Paolini, S., Pasquarello, A., Paulatto, L., Sbraccia, C., Scandolo, S., Sclauzero, G., Seitsonen, A.P., Smogunov, A., Umari, P., Wentzcovitch, R.M., 2009. QUANTUM ESPRESSO: a modular and open-source software project for quantum simulations of materials. *J. Phys.: Condens. Matter* 21, 395502.
- Hofmeister, A.M., 2006. Is low-spin Fe<sup>2+</sup> present in Earth's mantle? *Earth Planet. Sci. Lett.* 243, 44–52.
- Hsu, H., Umemoto, K., Cococcioni, M., Wentzcovitch, R., 2009. First-principles study for low-spin LaCoO<sub>3</sub> with a structurally consistent Hubbard  $U$ . *Phys. Rev. B* 79, 125124.
- Hsu, H., Umemoto, K., Wu, Z., Wentzcovitch, R.M., 2010. Spin-state crossover of iron in lower-mantle minerals: Results of DFT +  $U$  investigations. *Rev. Mineral Geochem.* 71, 169–199.
- Jackson, J.M., Sturhahn, W., Shen, G., Zhao, J., Hu, M.Y., Errandonea, D., Bass, J.D., Fei, Y., 2005. A synchrotron Mössbauer spectroscopy study of (Mg, Fe)SiO<sub>3</sub> perovskite up to 120 GPa. *Am. Mineral.* 90, 199–205.
- Kulik, H., Cococcioni, M., Scherlis, D.A., Marzari, N., 2006. Density functional theory in transition metal chemistry: a self-consistent Hubbard  $U$  approach. *Phys. Rev. Lett.* 97, 103001.
- Li, J., Struzhkin, V., Mao, H., Shu, J., Memeley, R., Fei, Y., Mysen, B., Dera, P., Pralapanka, V., Shen, G., 2004. Electronic spin state of iron in lower mantle perovskite. *Proc. Natl. Acad. Sci.* 101, 14027–14030.



- Li, J., Sturhahn, W., Jackson, J.M., Struzhkin, V.V., Lin, J.F., Zhao, J., Mao, H., Shen, G., 2006. Pressure effect on the electronic structure of iron in (Mg, Fe)(Si, Al)O<sub>3</sub> perovskite: a combined synchrotron Mössbauer and X-ray emission spectroscopy study up to 100 GPa. *Phys. Chem. Minerals* 33, 575–585.
- Lin, J.-F., Tsuchiya, T., 2008. Spin transition of iron in the earth's lower mantle. *Phys. Earth Planet. Inter.* 170, 248–259 and references therein.
- Lin, J.-F., Watson, H., Vanko, G., Alp, E.E., Prakapenka, V.B., Dera, P., Struzhkin, V., Kubo, A., Zhao, J., McCammon, C., Evans, W.J., 2008. Intermediate-spin ferrous iron in lowermost mantle post-perovskite and perovskite. *Nature Geosci.* 1, 688–691.
- Madsen, G., Blaha, P., Schwarz, K., Sjoestedt, E., Nordstroem, L., 2001. Efficient linearization of the augmented plane-wave method. *Phys. Rev. B* 64, 195134.
- McCammon, C., Kantor, I., Narigina, O., Rouquette, J., Ponkratz, U., Sergueev, I., Mezouar, M., Prakapenka, V., Dubrovinsky, L., 2008. Stable intermediate-spin ferrous iron in lower-mantle perovskite. *Nature Geosci.* 1, 684–687.
- Murad, E., Wagner, F.E., 1987. The Mössbauer spectrum of almandine. *Phys. Chem. Minerals* 14, 264–269.
- Narigina, O., Mattesini, M., Kantor, I., Pascarelli, S., Wu, X., Aquilanti, G., McCammon, C., Dubrovinsky, L., 2009. High-pressure experimental and computational XANES studies of (Mg, Fe)(Si, Al)O<sub>3</sub> perovskite and (Mg, Fe)O ferropericlae as in the Earth's lower mantle. *Phys. Rev. B* 79, 174115.
- Perdew, J.P., Burke, K., Ernzerhof, M., 1996. Generalized gradient approximation made simple. *Phys. Rev. Lett.* 77, 3865–3868.
- Petrilli, H.M., Blöchl, P.E., Blaha, P., Schwarz, K., 1998. Electric-field-gradient calculations using the projector augmented wave method. *Phys. Rev. B* 57, 14690–14697 and references therein.
- Stackhouse, S., Brodolt, J.P., Price, G.D., 2007. Electronic spin transitions in iron-bearing MgSiO<sub>3</sub> perovskite. *Earth Planet. Sci. Lett.* 253, 282–290.
- Sturhahn, W., Jackson, J.M., Lin, J.-F., 2005. The spin state of iron in mineral of Earth's lower mantle. *Geophys. Res. Lett.* 32, L12307.
- Tsuchiya, T., Tsuchiya, J., Umemoto, K., Wentzcovitch, R., 2004. Phase transition in MgSiO<sub>3</sub> perovskite in the earth's lower mantle. *Earth Planet. Sci. Lett.* 224, 241–248.
- Tsuchiya, T., Wentzcovitch, R., de Silva, C.R.S., de Gironcoli, S., 2006. Spin transition in magnesiowüstite in Earth's lower mantle. *Phys. Rev. Lett.* 96, 198501.
- Umemoto, K., Wentzcovitch, R., Yu, Y., Requist, R., 2008. Spin transition in (Mg, Fe)SiO<sub>3</sub> perovskite under pressure. *Earth Planet. Sci. Lett.* 276, 198–206.
- Umemoto, K., Hsu, H., Wentzcovitch, R.M., 2009. Effect of site degeneracies on the spin crossovers in (Mg, Fe)SiO<sub>3</sub> perovskite. *Phys. Earth Planet. Inter.* doi:10.1016/j.pepi.2009.10.014.
- Vanderbilt, D., 1990. Soft self-consistent pseudopotentials in a generalized eigenvalue formalism. *Phys. Rev. B* 41, 7892–7895.
- Wentzcovitch, R., Martins, J.L., Price, G.D., 1993. *Ab initio* molecular dynamics with variable cell shape: application to MgSiO<sub>3</sub>. *Phys. Rev. Lett.* 70, 3947–3950.
- Yu, Y., Wentzcovitch, R., Tsuchiya, T., 2007. First principles investigation of the postpinel transition in Mg<sub>2</sub>SiO<sub>4</sub>. *Geophys. Res. Lett.* 34, L10306.
- Yu, Y., Wu, Z., Wentzcovitch, R., 2008.  $\alpha$ - $\beta$ - $\gamma$  transformations in Mg<sub>2</sub>SiO<sub>4</sub> in Earth's transition zone. *Earth Planet. Sci. Lett.* 273, 115–122.
- Zhang, F., Oganov, A.R., 2006. Valence state and spin transitions of iron in Earth's mantle silicates. *Earth Planet. Sci. Lett.* 249, 436–443.